A Compact Magnetic Field Cloaking Device

A Thesis presented

by

Raphael Cervantes

to

The Graduate School

in Partial Fulfillment of the

Requirements

for the Degree of

Master of Science

in

Instrumentation

(Physics)

Stony Brook University

August 2015

Stony Brook University

The Graduate School

Raphael Cervantes

We, the thesis committee for the above candidate for the

Master of Science degree, hereby recommend

acceptance of this thesis

Dr. Abhay Lalit Deshpande
Professor, Department of Physics and Astronomy

Dr. Klaus Dehmelt
Research Professor, Department of Physics and Astronomy
Dr. Nils Feege
Postdoctoral Researcher, Department of Physics and Astronomy

Dr. Axel Drees
Professor, Department of Physics and Astronomy
Dr. Dominik Schneble
Associate Professor, Department of Physics and Astronomy
Dr. Matthew Dawber
Associate Professor, Department of Physics and Astronomy

This thesis is accepted by the Graduate School

Charles Taber
Dean of the Graduate School

A Compact Magnetic Field Cloaking Device

by

Raphael Cervantes

Master of Science

in

Instrumentation

(Physics)

Stony Brook University

2015

The proposed Electron Ion Collider (EIC) aims to deepen our understanding of quantum chromodynamics by measuring in detail the structure of protons and heavy ions. The EIC will collide hadrons and electrons with a momentum ratio of 12:1, resulting in a large number of particle debris in the forward direction of the interaction region. Employing a magnetic field orthogonal to the beam line is optimal for momentum spectrometry, but the collider beam must be shielded from this field to avoid deflection and depolarization. We develop a magnetic cloak to address this issue. Such a device creates a field free tunnel inside a magnetic field without disturbing it outside, enabling significantly improved momentum resolution for particles produced from collisions compared to the conventional solenoidal magnet.

Dedication Page

To my dear grandmother Josefina.

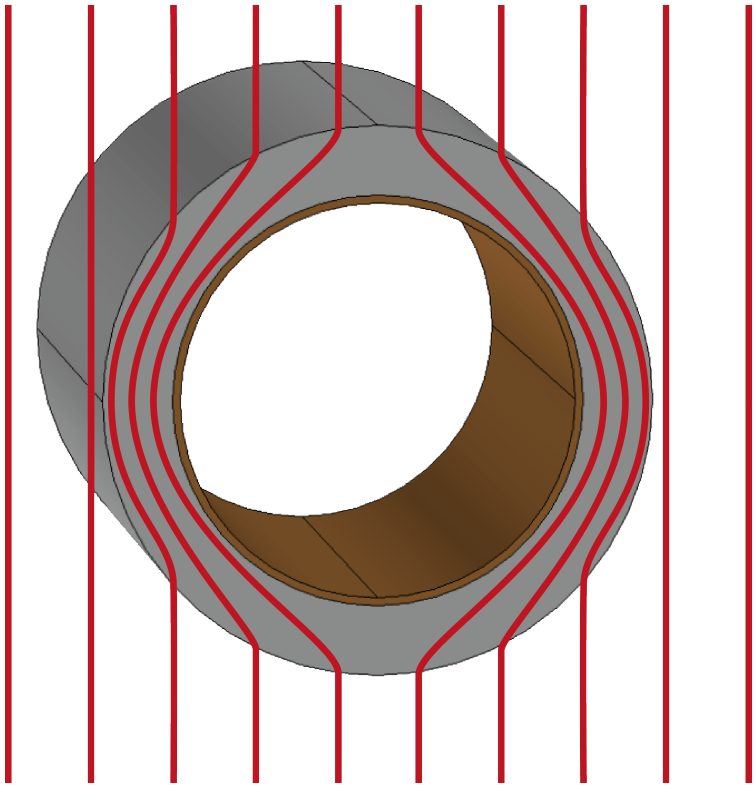

Table of Contents

Contents

List of Figures

Acknowledgements

I thank my advisor Professor Abhay Deshpande for his guidance during a period of existential uncertainty. It was through his support that I figured out what I wanted to do with my life. I thank him for being confident in me when I lacked confidence.

I thank Dr. Nils Feege for his guidance and for tolerating my stubbornness and "negativity" throughout the entire project. I think we complimented each other well. He probably disagrees.

I thank the thesis committee for scheduling my thesis presentation on short notice.

I thank the EIC R&D Program for continuously funding this project.

I thank the EIC R&D Advisory Committee for reviewing our progress and asking important questions that need to be addressed for us to realize success.

I thank Ramesh Gupta and William Sampson from the BNL Superconducting Magnet Division for their guidance in the superconductor aspect of our project.

I thank Rob Rouse from American Superconductors for providing us with the 46 mm wide tape, even though it was not commercially available. This contribution was vital to the success of our project.

I thank SuperPower Inc. for also providing with superconductor. This contribution was vital for our initial measurements.

I thank LakeShore for their expertise in Hall sensors.

I thank Richard Lefferts and Andzrej Lipski for their guidance in designing our experiments.

I thank Ernest Ihloff for providing us with the necessary power supply.

I thank the undergraduates in our lab. I'll keep this particular acknowledgement general for fear of misattributing or forgetting individual contributions. However, this project wouldn't have made as much progress as it has without their efforts. The scientific community appreciates their mostly unpaid labor and I wholeheartedly sympathize with them.

I thank my family for loving me even after being away from home for so long.

I thank my friends back home. They help me remember where I came from and how far I've come, among other things.

I thank my teacher Robert Morris for fostering my academic growth at a time when I needed it most. I just wish he would stop reminding me of my poor dating experiences.

I thank my former advisors Professor Peter Fisher and Professor Nergis Mavalvala for helping me grow into the experimentalist that I am today. I sincerely apologize for frustrating them with my carelessness and poor time management skills.

Honestly, I am thankful for everyone who has given me new insights into life. Thanks for enriching my life experience and helping me become a better version of myself.

1 Introduction and Motivation

1.1 The Case for an Electron Ion Collider

Within the past few decades, we have learned much about the matter that constitutes the visible universe. With a better understanding of these building blocks comes a better understanding of the physical laws that govern them. For example, the discovery that matter was made out of atoms consisting of protons, neutrons, and electrons led to a better understanding of chemistry and the development of quantum mechanics. Likewise, the discovery that nucleons consisted of quarks and gluons led to the development of quantum chromodynamics (QCD). Particle colliders have provided us the tool to understand nuclear structure. By analyzing the byproducts of particle collisions, we can gain insights into the structure of subatomic particles, and the physics that governs them.

Although current particle colliders have helped us learn more about nuclear structure and QCD, many questions remain unanswered. First, the origin of the proton's spin remains a mystery. Experiments have shown that the intrinsic spin of the quarks only contributes $\approx 30\%$ of the total spin, and that the gluon's intrinsic spin is not enough to account for the remaining 70% [1, p. 2]. Second, we have not measured gluon density saturation. So far, the deeper we have probed into the nucleus, the more gluons we have seen. However, we cannot observe an infinite gluon density, so there must be a point in which the gluon density saturates. Studying this Color Glass Condensate phase of matter will give us deeper insights into the strong force [1, p. 7].

The Electron-Ion Collider (figure 1a) will be equipped to answer these questions. Electron-hadron collisions are much cleaner than hadron-hadron collisions, as electrons are structureless particles that will only react electromagnetically instead of through the strong force. The colliding electron will interact with the individual quarks and gluons, allowing us to measure their spatial and momentum distribution in the proton (figure 1b). Polarized proton and electron beams will be essential to measuring spin structure. Heavy ion beams are needed to understand physics at saturated gluon densities [1, p. 2].

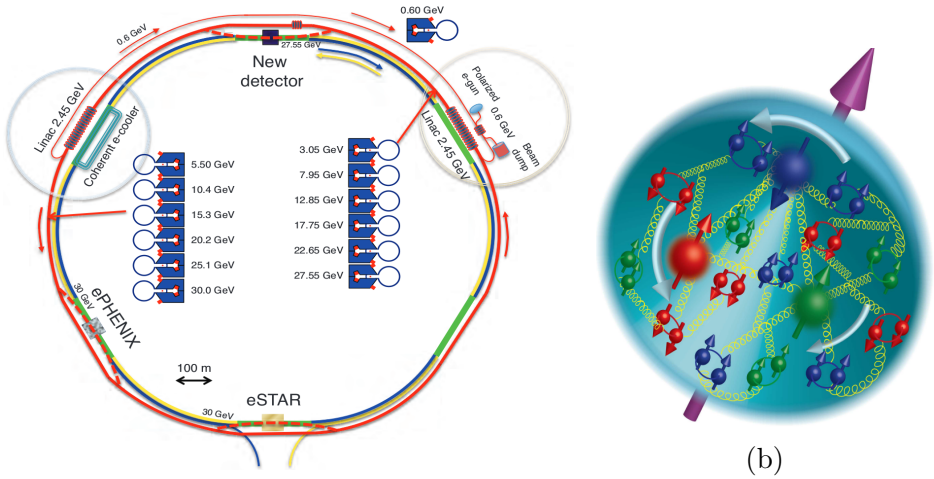

(a) (b)

Figure 1: (a) Current design for constructing the EIC at BNL. (b) One of EIC's physics deliverables is to gain a better spatial and momentum image of the proton's quarks and gluons [1, p. 3,12].

1.2 The Case for a Forward Dipole Magnet Analyzer in an EIC Detector

Magnetic fields are an integral part of accelerator based experiments. These fields cause the trajectory of charged particles to bend according to the Lorentz force, $\mathbf{F} = q[\mathbf{E} + (\mathbf{v} \times \mathbf{B})]$. By placing the particle detector in a magnetic field, we can determine a charged particle's momentum by measuring its altered trajectory.

Momentum spectrometry becomes difficult in electron-ion collisions due to the momentum asymmetry[1]. Because of the momentum asymmetry in the colliding beams, the trajectory of the debris will be heavily skewed towards the proton-going direction (figure 2, 3)[2]. Since the debris will be nearly parallel to the standard solenoid field, the resulting particles will receive minimal deflection, leading to poor momentum resolution.

[1]The momentum asymmetry is necessary because we cannot radially accelerate an electron to as high of an energy as an ion due to the electron losing a lot of energy to synchrotron radiation.

[2]Pseudorapidity η describes the angle of a particle relative to the beam axis and is defined as $\eta \equiv -ln[tan(\theta/2)$. It is preferred over the polar angle θ because it allows for Lorentz invariant calculations.

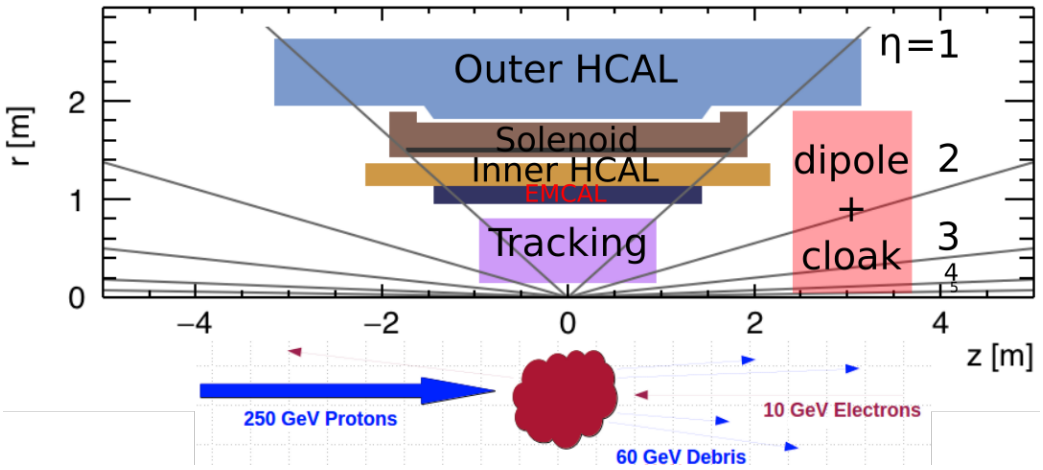

Figure 2: Schematic of a detector experiment. Placing a combination of a dipole magnet and magnetic cloak can increase the momentum resolution in $2 < \eta < 4$.

One solution would be to place a magnetic field perpendicular to the beam axis. Thus, particles going in the forward direction would experience a magnetic field nearly perpendicular to their trajectories. The orthogonality of the field leads to more deflection, and thus better momenta resolution. Figure 4 demonstrates the improved momentum in the high η regime by adding a 0.5 T dipole magnet to a 1.5 T solenoid magnet. Details of the calculation can be found in the appendix A.

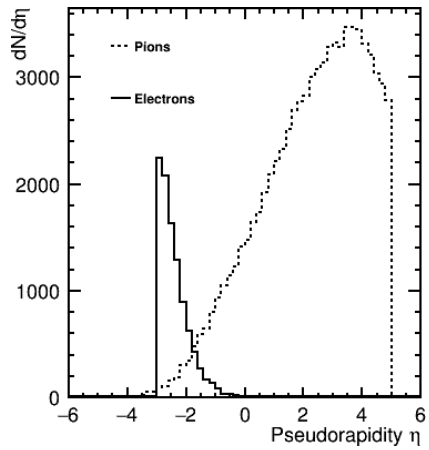

Figure 3: The η distribution of the resulting pions and electrons from 10,000 Deep Inelastic Scattering events (with a cut on the square 4-momentum transfer $Q^2 > 1$ GeV). Most of the hadron debris and final state electrons are concentrated in the very forward region of the detector ($|\eta| > 2$).

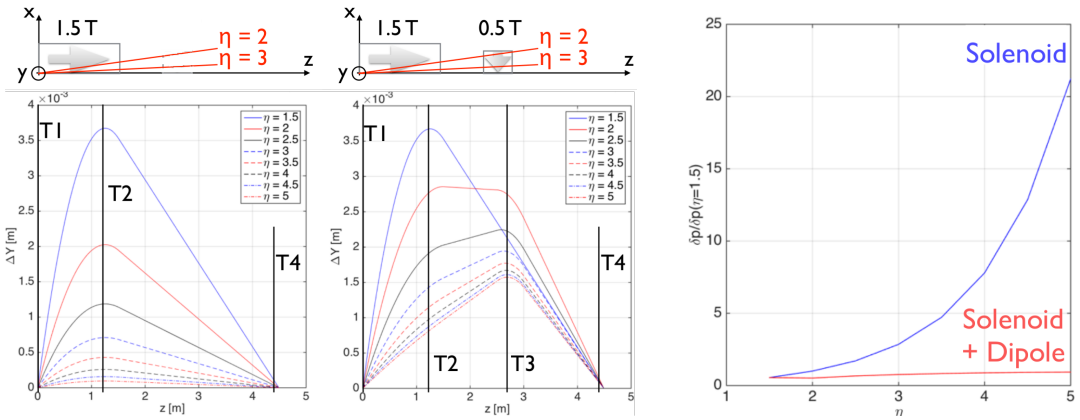

(a) (b)

Figure 4: (a) Calculate track bending of 50 GeV particles with different η for a 1.5 T solenoid magnet combined with a 0.5 T dipole magnet in the forward direction. T1, T2, T3, and T4 are tracking stations that allow measurement of the maximum trajectory bending.(b) Momentum resolution δp calculated with tracking spatial resolution $r\delta\varphi \sim 100\mu m$. The results are normalized to $\delta p(1.5\eta)$. Adding the dipole magnet significantly reduces the momentum uncertainty for particles with $\eta > 2$

1.3 The Case for a Magnetic Cloak around a Beamline

Unfortunately, a magnetic field perpendicular to the initial particle beam would deflect and depolarize it, thus ruining the physics one wanted to measure in the first place. To make the use of a dipole magnet possible, we propose the implementation of a magnetic field cloaking device. A magnetic cloaking device creates a region free of magnetic fields inside of it without disturbing the magnetic fields outside. This behavior contrasts with superconductor or mu-metal shields, which shield the internal volume at the expense of distorting the field around it.

We can achieve cloaking in a cylindrical volume by using a superconductor/ferromagnet bilayer. The superconductor creates currents that prevent field from entering its volume. Although the inside of the superconducting tube is field-free, the field on the outside has been pushed out. We can compensate for this field disturbance by adding a ferromagnetic layer. The ferromagnet has the opposite effect; instead of pushing away magnetic fields, it pulls them inward. By combining the pushing of the superconductor with the pulling of the ferromagnet, we can cancel both opposing effects to maintain a homogeneous field outside of the bilayer. To achieve this perfect cancellation of distortion effects, the magnetic permeability of the ferromagnet must be

$$\mu_r = \frac{R_2^2 + R_1^2}{R_2^2 - R_1^2}, \tag{1}$$

where R_1 and R_2 are the inner and outer radii of the ferromagnet, respectively [2].

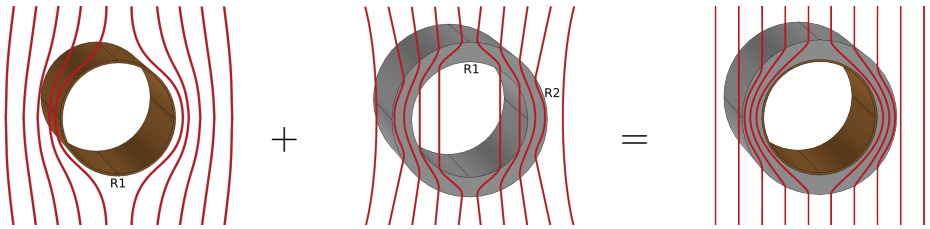

(a) Superconductor (b) Ferromagnet (c) Magnetic Cloak

Figure 5: A conceptual magnetic cloak made from a superconductor/ferromagnet bilayer. The red lines indicate the magnetic field lines.

1.4 Experimental Realization of a Magnetic Cloak

Efforts are currently ongoing to realize a magnetic cloaking device suitable for the needs of the EIC. Such a cloak would have to be 1 m long and shield a 0.5 T transverse field. Over the past year, significant progress has been made to make such a device using commercially available material. Section 2 describes current efforts to make a superconductor layer scalable in both field and length. Section 3 describes our efforts to build a ferromagnet layer that meets the conditions of equation 1. Section 4 describes the results of our cloaking prototype. Section 5 describes ongoing efforts to test our cloak prototype in accelerator conditions.

2 Superconductor Studies

A magnetic cloak consists of an inner superconductor layer and an outer ferromagnet layer. The superconductor layer's purpose is to prevent fields from penetrating the cloak's volume, thus isolating the interior from external fields. Superconductors repel fields by inducing currents that create a counter-field which cancels out the applied field, up to a critical field. Fields beyond this threshold seep through[3]. To increase the amount of field that the layer can shield, we should choose the superconductor with the highest intrinsic critical field. We can also stack an arbitrary number of layers together to achieve the overall critical field we require[4].

2.1 Choice of Superconductor

Our choice of superconductor must shield at least 0.5 T field through 1 m of beampipe in accelerator conditions. We have explored the following options:

1. Low-temperature superconductor with Niobium-Titanium: NbTi/Nb/Cu sheets have been demonstrated to shield magnetic fields of 1 T and above. However, NbTi has critical temperature of $\approx$ 9K, and therefore requires liquid helium cooling. Another caveat is that these sheets are also no longer being produced and only a few remaining sheets are available from the supplier[5].

2. Medium-temperature superconductor with Magnesium Bromide: A recent paper showed that a 10 cm MgB_2 tube can shield up to 2 T at a temperature of 4.2 K[4]. Because the critical temperature of this material is 39 K, the requirements for the cryogenic cooling system are less stringent than for NbTi. To obtain cylinders made from this superconductor, we would have to sinter it in-house. Obtaining the raw materials and sintering a 10 cm prototype is feasible. However, we do not have a furnace long enough to produce a 1 m prototype.

[3]The reader is encouraged to study appendix C to understand how type-II superconductors work.

[4]Actually, stacking superconductors will only work as long as the applied field remains below the second critical field ($\sim$ 10 T for YBCO).

[5]As far as we are aware, Nippon Steel is the only manufacturer that has made NbTi sheets for shielding applications[3].

3. High temperature superconducting ceramic tubes[5]: High temperature superconductors can operate at liquid nitrogen temperatures. The relaxed cryogenic constraints vastly simplify testing. Unfortunately, commercially available tubes are limited in length and diameter. We cannot realistically achieve 0.5 T shielding by layering one tube inside another since each layer is 1.5 mm thick and can shield only up to 10 mT.

4. High-temperature superconductor tape: We can wrap this tape around the beam pipe to shield the pipe from magnetic fields. This option has the most relaxed cryogenic requirements and and most flexibility in length and diameter that it can shield. The biggest disadvantage is the limited width of the tape. The commonly available 12 mm wide tape cannot sufficiently shield a beam pipe 2 cm in diameter. One cannot wrap such a pipe with this narrow tape without gaps in between superconductors. Our measurements show that covering these gaps with more superconductor (figure: 6 and 8a) is not a viable solution for shielding 0.5 T.

   We also obtained a sample of 46 mm wide superconductor tape from American Superconductors. This width is not commercially available at the moment- it is an intermediate state of the tape on their production line[6]. This tape allows us to wrap two half-tubes around a 1" core. This configuration allows the supercurrents to act like a cos-theta magnet and is therefore very effective for shielding transverse magnetic fields (figure 7)[7]. Also, forming a long superconducting cylinder using shells from 46 mm wide tape is far easier to do and less error prone than wrapping 12 mm tape helixes. However, this configuration limits the maximum diameter of the cylinder that two strips of this tape can cover.

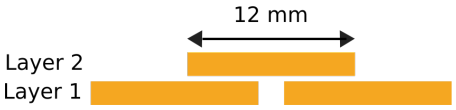

Figure 6: 12 mm wide superconducting tape wrapped helically around a copper tube. Each turn of the helix results in a gap between superconductor, so we used the next layer to cover the gap.

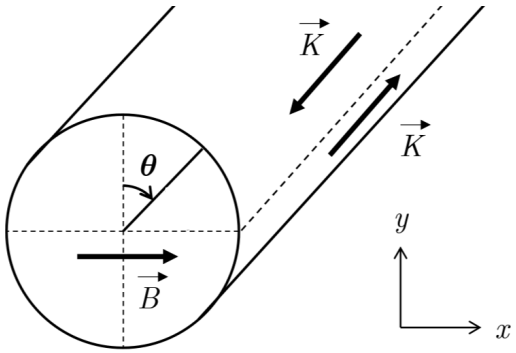

Figure 7: A cosθ magnet with a continuous surface current distribution $\mathbf{k} = kcos\theta\hat{z}$. $\mathbf{k}$ creates a magnetic field transverse to the magnet[7].

2.2 Method of Characterizing Superconductor Performance

We tested the shielding capabilities of both 46 mm wide tape from American Superconductors and the 12 mm wide tape from Superpower. First, we wrapped the superconducting tape around a 1" copper core to make a superconducting tube (figure: 8a). For the 46 mm wide tape, we only needed to use two strips of superconductor to cover both sides of the core. We left an overlap where the two strips met to cover any superconducting gaps. We could not cover half the core with the 12 mm tape, so we wrapped it helically. We covered the superconducting gaps of one layer with the layer on top (figure 6).

We then placed each superconducting tube in a Helmholtz coil and measured the amount of the transverse field that leaked through (figures: 8b, 8c). The superconductors were first cooled in a mu-metal canister to avoid trapping stray fields. The superconductor tube, while still in its liquid N_2 bath, was moved inside the Helmholtz coil. The Hall probe slides vertically through an 80/20 t-slot frame. We placed the Hall probe at the center of the superconducting tube, allowing us to measure the field leakage as a function of the

applied field[6]. In other experiments, we fixed the applied field and measured the leakage through the length of the superconductor.

We also measured the intrinsic shielding properties of the 12 mm wide tape, without the effects of superconducting gaps. To accomplish this, we sandwiched the Hall probe in between two superconducting strips (a superconducting sheath, figure: 9a). To the Hall probe, this would effectively be a nearly infinite plane.

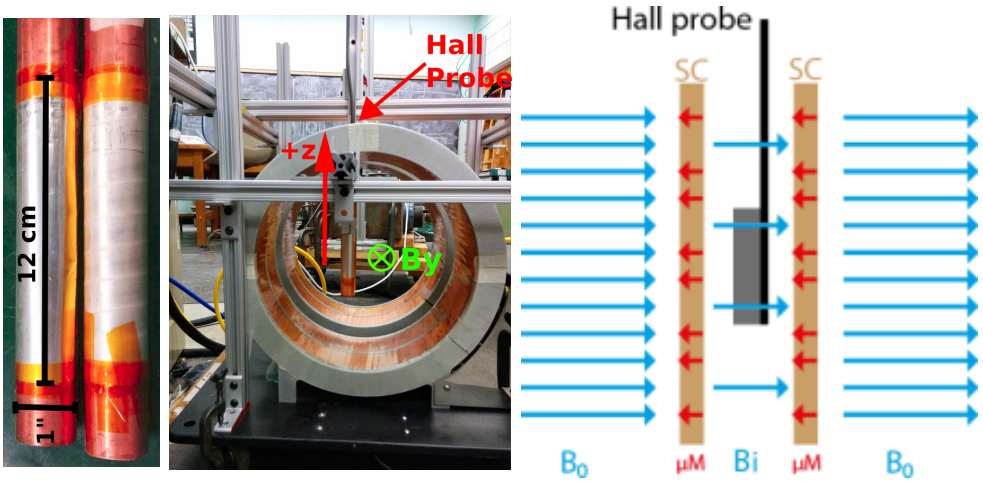

(a) (b) (c)

Figure 8: Experimental setup to measure shielding properties of the superconductor tape. (a) We formed the tape into superconducting tubes. (b) Each tube was placed in a magnetic field to measure its shielding properties. (c) We used a Hall probe to measure the leaking field B_i as a function of the applied field B_o.

2.3 Characterizing SC Tape

First, we determined if 12 mm wide tape could realistically shield 0.5 T. Figure 9b shows that the tape could realistically shield about 20 mT. Unfortunately, we saw significantly worse shielding when we tried to wrap a core

[6]There is a time dependence to the leaked field. Other experiments take this measurement while constantly ramping the applied field[8, 9] We are interested in the long-term behavior, so we extrapolated B_i to half a year. See appendix D for more details

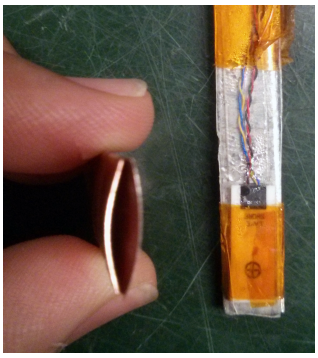

(a)

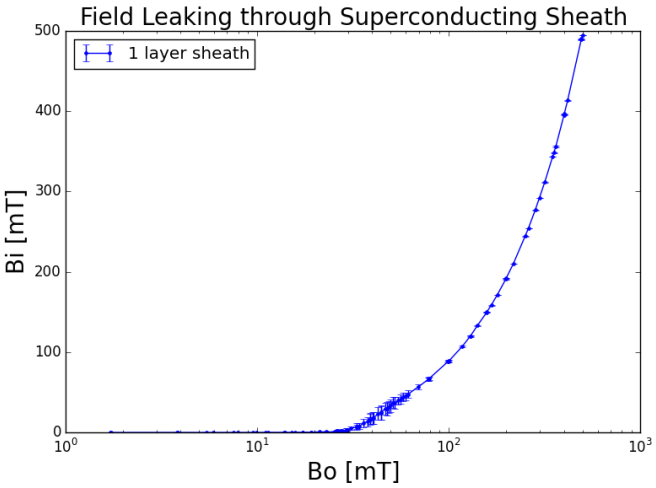

(b)

Figure 9: (a) We encased the Hall probe in a superconducting sheath (two strips of 12 mm wide superconductor) to measure its intrinsic shielding properties. (b) Measurement of the field that leaks through the superconducting sheath. The sheath measurement showed that the 12 mm wide Superpower tape can shield about 20 mT.

12 cm in length and $\approx$ 1" in a diameter. As stated before, one cannot wrap such a pipe with this narrow tape without gaps in between superconductors (figure: 8a). The field seeps through in between the superconducting turns, as can be seen from the undulations in the 1 layer measurement (figure 12a). We covered these gaps with each subsequent layer. We also tried to get the superconductor as close as possible with the 'adjacent wrapping' (figure 10b) and by wrapping tape without the copper stabilizer (figure 10c). Unfortunately, these different wrapping styles only provided a marginal increase in shielding (figure 11). Ultimately, 5 layers of the 12 mm tape could only shield about 12 mT. It would require an unreasonable number of layers to shield 0.5 T, so we concluded that 12 mm wide tape was not a viable option.

From figure 13a, we see that 1 layer of the 46 mm wide tape performed better than 5 layers of the 12 mm wide tape at an applied magnetic field of $B_o > 15$ mT, despite the better intrinsic shielding properties of the 12 mm wide tape, as derived from the sheath geometry measurement. This suggested that the 12 mm wide tape has a higher critical current than the 46

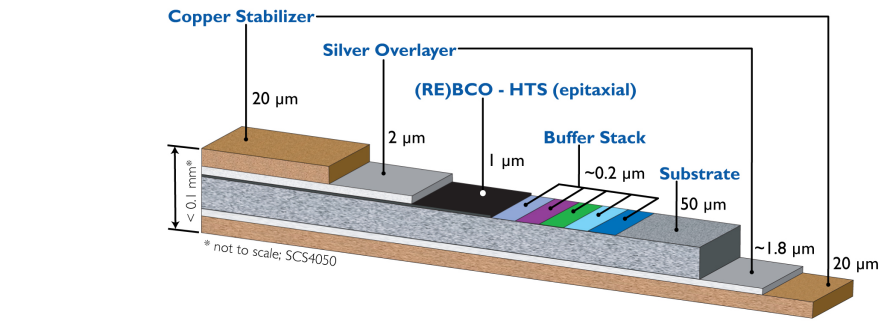

(a)

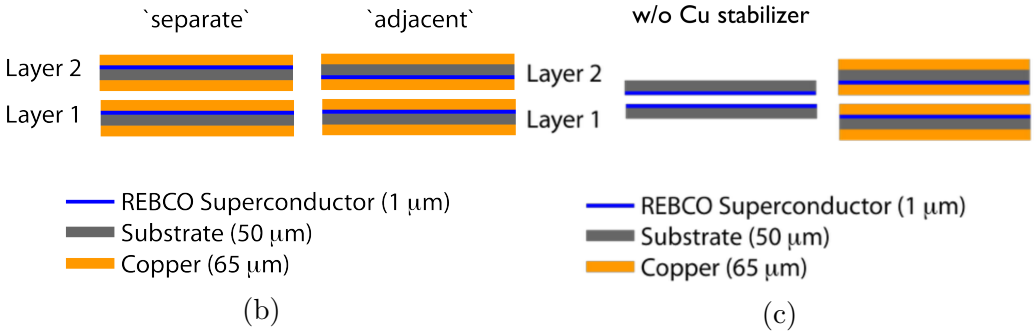

(b) (c)

Figure 10: (a) Structure of the Superpower tape. The REBCO superconductor lies closer to one side of the tape than to the other. (b) Method of decreasing superconducting gaps by having the superconducting sides face each other ('adjacent' configuration). (c) Attempt to decrease superconductor gaps even more by wrapping tape without copper stabilizer.

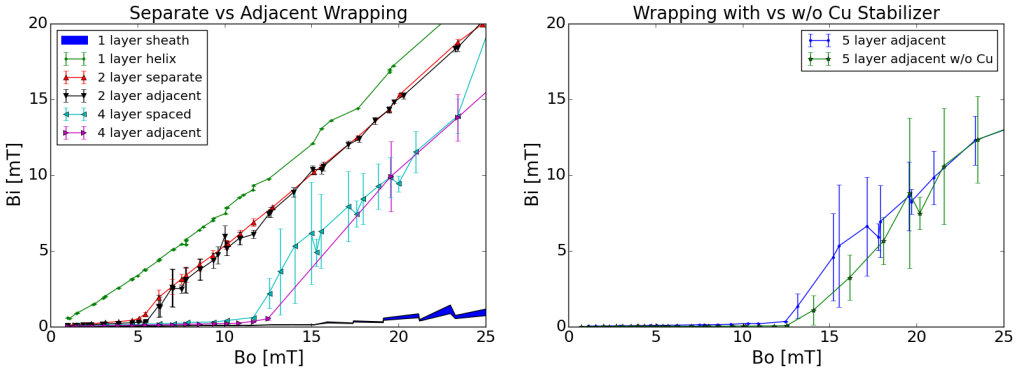

(a) (b)

Figure 11: (a) Measurement of the field leaking through different superconductor wrapping configurations (figure 10). The measurement for a small sheath of the tape is included for reference. (b) Comparison of superconducting cylinders made from 5 layers of tape (helix, adjacent) with and without copper stabilzer. Getting the superconducting material between layers closer together only provided marginal improvement.

mm wide tape. But a higher critical current is not enough to shield higher fields; we must also allow the supercurrents to flow in a path that allows for shielding of the applied field. The current flow in the helical winding is interrupted by the gaps. Thus, the 46 mm wide tape performed better due to its geometry rather than its critical current.

From the single layer measurement, we extrapolated the shielding capabilities of an arbitrary number of layers, up to the maximum field measured by the first layer. We performed this extrapolation by stating that the applied field on the 2nd layer is the leaked field from the 1st layer. We can iterate this procedure to obtain the shielding performance of an arbitrary number of layers. Figure 13b shows that our measurements were in great agreement with the extrapolated predictions.

The Helmholtz coil can only reach about 55 mT, so we used a dipole magnet to characterize the superconductor at higher fields. The dipole magnet is not ideal due to its inhomogeneity, but is good enough to characterize 1 layer. We measured the shielding of 1 layer up to 0.5 T, and extrapolated to an arbitrary number of layers. We see from figure 13c that we can shield 0.5 T with about 40 layers of superconductor. While this number seems high, it

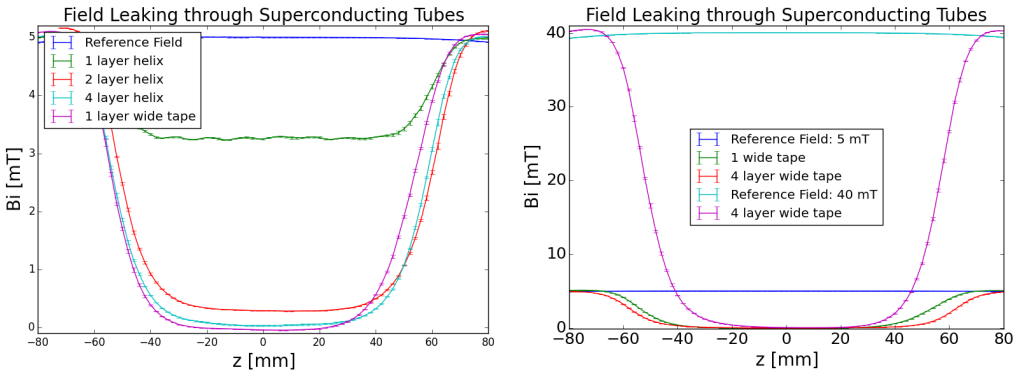

(a) (b)

Figure 12: (a) The transverse field measured inside superconducting cylinders placed inside a homogeneous external field of 5 mT as a function of the position along the center axis of these cylinders. The undulations in the leaked field through the 1 layer helix wrapping demonstrated that the field leaks through the gaps. The undulations disappeared for multiple layers, but the shielding still suffered. Just 1 layer of the wide tape outperformed 4 layers of the narrow tape. (b) The shielding performance of the wide tape superconductor tubes. The fringe effects were reduced by increasing the number of layers. The higher the field, the stronger the fringe effects were.

is comparable to the number of layers in a commercial NbTi sheet[10].

We can reduce the number of layers needed by going to liquid Helium temperatures. We estimated that a temperature of 4.2 K allows us to shield 0.5 T with only 11 layers, as shown in figure 13d. This estimate assumes that the shielding performance scales with the increase in critical field at lower temperatures, such that

$$B_i(B_o, T = 4.2K) = B_i(\frac{B_c(T = 77K)}{B_c(T = 4.2K)} \times B_o, T = 77K).$$

We would have to do a measurement to confirm this prediction. Table 1 compares the thickness of the three shielding options: NbTi, HTS wide tape with liquid nitrogen, and HTS wide tape with liquid helium. It has not been decided whether the reduction in thickness is worth the cryogenic complications of liquid helium.

Table 1: Superconductor options to shield 0.5 T transverse field

Superconductor	Cooling	Layers	Thickness [mm]
NbTi/Nb/Cu	lHe	1	1
AMSC SC 46 mm	lHe	11	0.9
AMSC SC 46 mm	lN_2	45	3.6

We also measured the spatial dependence of the superconducting tubes' shielding capabilities (figure 12). We saw that fields leak into the superconductor through the ends. The higher the field, the more the field leaks through. Ref. [8] discusses an exponential relationship of the leaked field at the extremities of the tube. Beyond the fringe area, the field profile was relatively flat. Ref. [11, p.94] states that this plateau should exist if $l > 3$ OD_S, where l is the length of the diameter, and OD_S is the outer diameter of the superconductor. Nevertheless, these fringe effects can be mitigated by making the superconductor longer than the field.

We are excited to demonstrate the feasibility of shielding a 0.5 T magnetic field with high temperature superconductors. Such a feat is unprecedented to our knowledge, especially at liquid Nitrogen temperatures.

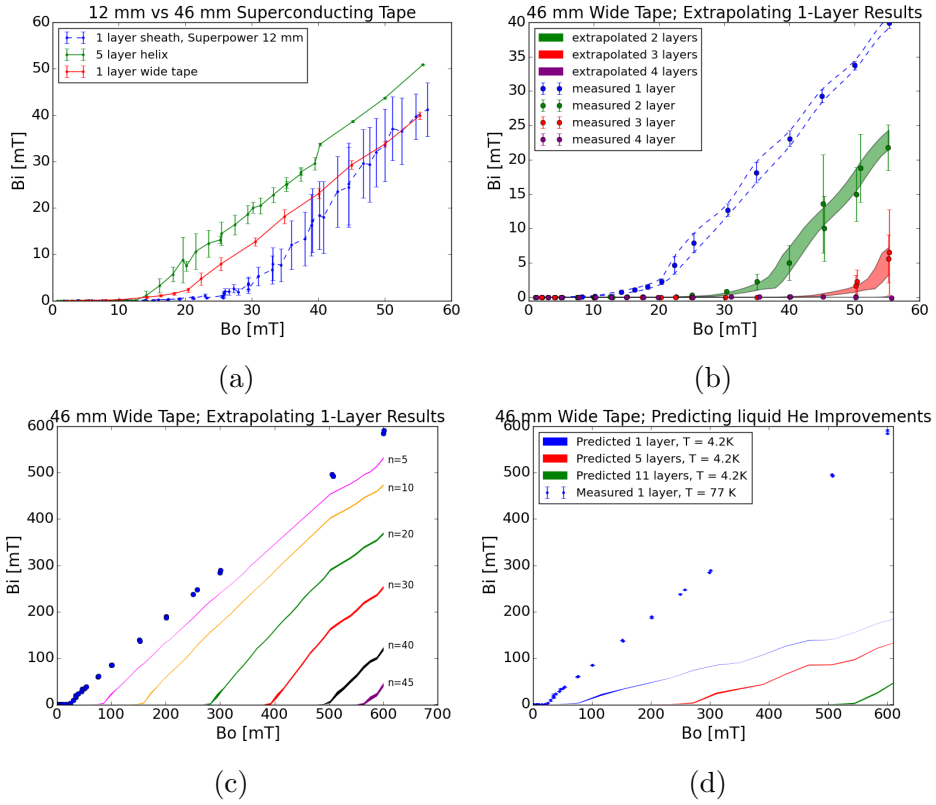

Figure 13: (a) The magnetic field inside a sheath of 12 mm SuperPower tape, a cylinder made from 5 layers of this tape, and a cylinder made from one layer of the wide tape, as a function of an externally applied field. The wide tape was better at shielding a 1 diameter tube than the 12 mm tape, although the 12 mm tape is of superior quality. (b) Measurements and predictions (based only on the 1-layer measurement) for the field inside superconducting cylinders made from 1, 2, 3, and 4 layers of the wide superconductor tape. The measurements for multiple layer shielding agreed very well with the predictions. (c) Shielding measurements with 1 layer sheath in a dipole magnet. Extrapolations (based only on the 1-layer measurement) predicted that 40 layers will shield 0.5 T. (d) Predicted shielding improvements by cooling the superconductor to liquid He temperatures (instead of liquid Nitrogen).

2.4 Conclusion

Our superconductor studies remain incomplete, but promising. We have demonstrated shielding up to 55 mT with high temperature superconductor tape. Our results in an inhomogeneous dipole magnet suggest that it will take 40 layers to shield 0.5 T at liquid nitrogen temperatures and 10 layers with liquid helium. To push forward, we must confirm these predictions with a 0.5 T homogeneous field.

3 Ferromagnet Studies

A magnetic cloak consists of an inner superconductor layer and an outer ferromagnet layer. While the superconductor layer isolates the cloak's interior to external fields, it distorts the external field on the outside by pushing out the field lines. Adding a ferromagnet layer cancels out this distortion by pulling in the magnetic fields.

3.1 Fabrication of Ferromagnet

Our ferromagnet must have a relative permeability and thickness that meets the conditions of equation 1. Most commercial materials have either $\mu_r = 1$ or $\mu_r > 100$. However, a ferromagnetic layer with an easily manufacturable thickness requires a permeability between 3 and 20. For example, a ferromagnetic layer of $R_1 = 2.5$ cm and $R_2 = 3$ cm needs $\mu_r \approx 5.5$ to be useful for a magnetic cloak. Figure 14 shows the relationship between the thickness of a ferromagnet and the ferromagnet's permeability. The higher the permeability, the thinner the ferromagnet can be. However, the larger slope at smaller thicknesses means that we are less tolerant to deviations to the cloaking permeability.

In response, we have established a procedure to mix ferromagnetic and non-ferromagnetic material to dilute the permeability in a precise manner. More specifically, ferromagnetic tubes were produced by mixing 430 stainless steel powder with commercial epoxy (figure 15). The mixture was poured into a tubular mold. Because stainless steel is much denser than epoxy, we rotated the epoxy constantly (by hand) while it was curing to avoid a gradient of fractional volume of epoxy along the length. By controlling the volume fraction of stainless steel powder in the epoxy, the permeability can be fine-tuned [12].

The physics controlling the effective permeability of mixtures is defined by the volume fraction [13]. But it is much easier to measure mass than it is to measure volume. For a desired fractional volume, the mass fraction can be calculated by the following equation:

$$\frac{m_{FM}}{m_E} = \frac{V_{FM}}{V_E}\frac{\rho_{FM}}{\rho_E} = \frac{V_T f}{V_T(1-f)}\frac{\rho_{FM}}{\rho_E} = \frac{f}{1-f}\frac{\rho_{FM}}{\rho_E}, \tag{2}$$

where f is the fractional volume of ferromagnet in ferretic epoxy, m is mass, V is volume, ρ is mass density, and the subscripts FM, E, T relate the mentioned

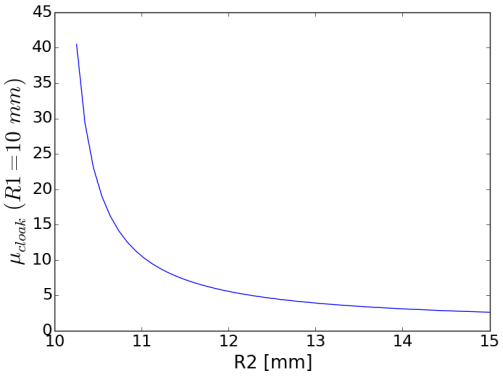

Figure 14: The required permeability as a function of outer radius R_2, given that $R_1 = 2$ cm.

(a) 430 Stainless Steel Powder, $\mu_r \simeq 500$

(b) Epoxy, $\mu_r = 1$

(c) FM Epoxy, $1 < \mu_r < 6$

Figure 15: We mix 430 stainless steel powder in epoxy and pour the mixture into a tubular mold. We can adjust the fractional volume of stainless steel powder to control the permeability.

variables to the ferromagnet, epoxy, and the total mixture, respectively. $f > 0.4$ was not possible as the resulting viscosity of the mixture was too high to pour into a mold.

3.2 Method of Characterizing Ferromagnets

We can measure the permeability of a ferromagnet tube of inner and outer radius R_1 and R_2 by measuring the internal field B_i as a function of the applied homogeneous field B_o. For a finite length ferromagnet, B_i will vary along the length, so we quote the measured μ_r in the center of the ferromagnet.

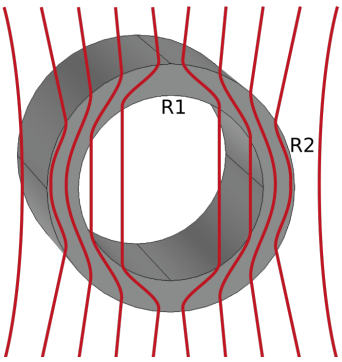

Figure 16: We can measure the μ_r of a ferromagnet tube by measuring how well it magnetically shields the interior. The higher μ_r, the less field reaches the interior.

$$\mathbf{B}_i(r < R_1) = \frac{4\mu_r R_2^2}{(\mu_r + 1)^2 R_2^2 - (\mu_r - 1)^2 R_1^2}\mathbf{B}_o, [14] \tag{3}$$

We can determine if the ferromagnetic powder is evenly distributed in the epoxy by measuring the interior field throughout its length. If it is evenly distributed, then the shielding profile should be symmetric and have a minimum at the center of the ferromagnet.

3.3 Permeability Measurements of Ferromagnets

Figures 17 and 18 demonstrate that the ferromagnetic epoxy has a significantly lower relative permeability than that of a 430 stainless steel sheet. Except for f=0.15, the samples' μ_r and required thickness are relatively stable up to a maximum measured applied field of 55 mT. We see a slight decrease in μ_r with higher fields, so it is necessary to measure the permeability at 0.5 T to determine the viability of using this ferromagnet for accelerator experiments.

A volume fraction of f = 0.4 is best suited for our needs. It has the highest permeability of the mixtures, thus leading to a thinner ferromagnet layer. Unlike the stainless steel sheets, the thickness is still easily machinable, e.g. R1 = 2 cm requires R2 $\approx$ 2.4 cm.

Figure 19 demonstrates a decrease in permeability when we perform the measurement in liuid nitrogen. This shift can be attributed to an increase

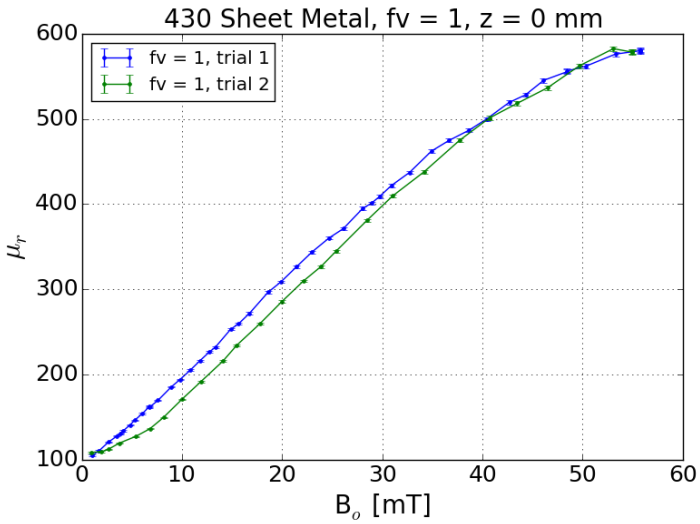

Figure 17: The measured permeability of a 430 stainless steel sheet as a function of applied field. The difference in the two trials can be attributed to hysteresis.

in the anisotropy constant[7] [15]. The permeability is expected to decrease further at liquid helium temperatures.

We also considered whether or not our method could scale up to develop 1 m prototype. It would be impractical to pour epoxy into a 1 m mold, so we considered whether or not we could stitch together smaller tubes and achieve the same magnetic properties. We tested this stitching method by cutting the ferretic epoxy tube in half and measuring its shielding profile after putting the two pieces back together. Figure 20 shows that making this cut made no difference in the position of the shielding profile's minimum. The offset between the cut and uncut profiles likely results from hysteresis. Regardless, the fact that the profile shape does not change shows that we can scale the length merely by stitching smaller tubes together.

[7]The magnetic anisotropy represents the energy needed to pull the magnetization away from the its preferred (easy) axis in the crystal structure. The higher the temperature, the more the magnetic domains "jitter" along an axis. This jittering reduces the energy difference between the domain being aligned along the easy axis and the domain being aligned with the hard axis.

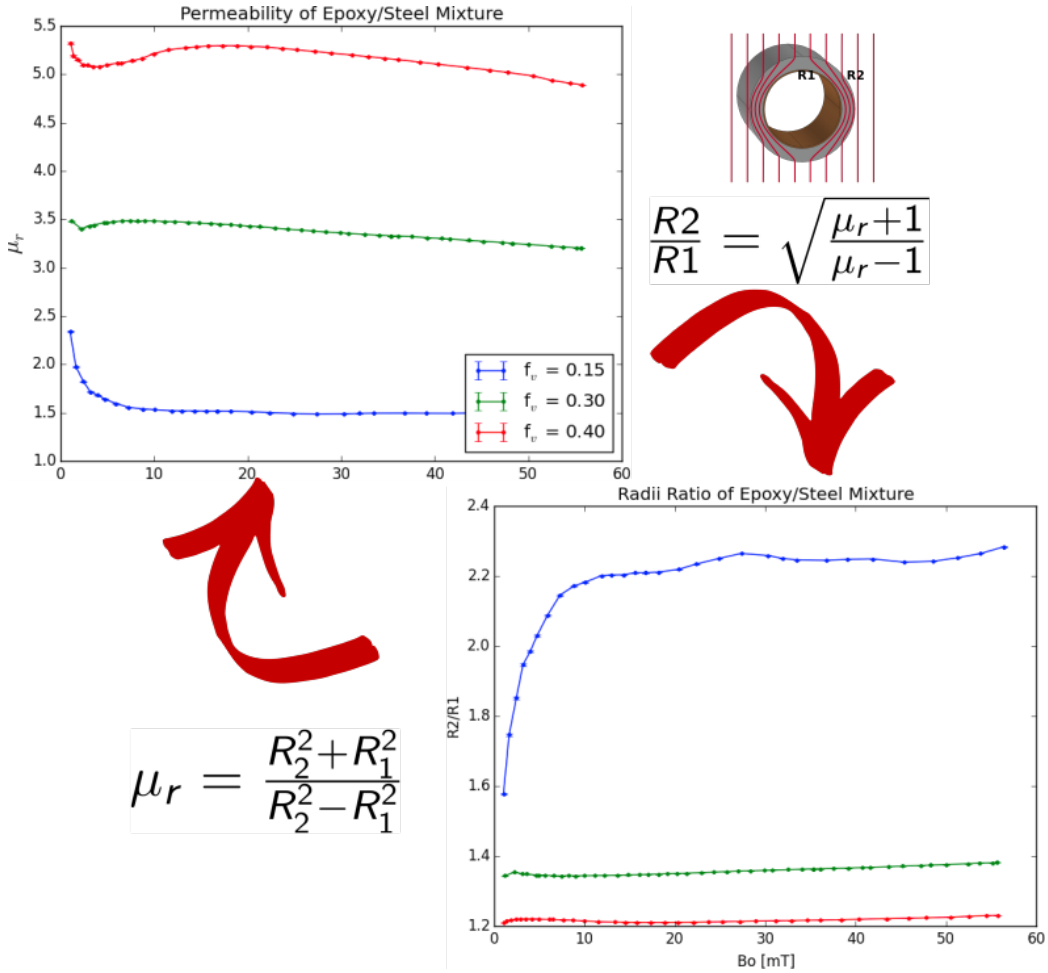

Figure 18: (Top) The measured permeability as a function of applied field for steel/epoxy mixtures of different fractional volumes. For each measured permeability, the ideal thickness of the ferromagnet was calculated. We measured the permeability as a function of applied field for steel/epoxy mixtures of different fractional volumes. From each measured permeability, we calculate the ideal geometry of the ferromagnet. We confirm that mixing ferromagnetic material in a non-magnetic medium dilutes the effective permeability. The ferromagnetic epoxies have a significantly reduced μ_r compared to the 430 stainless steel sheet.

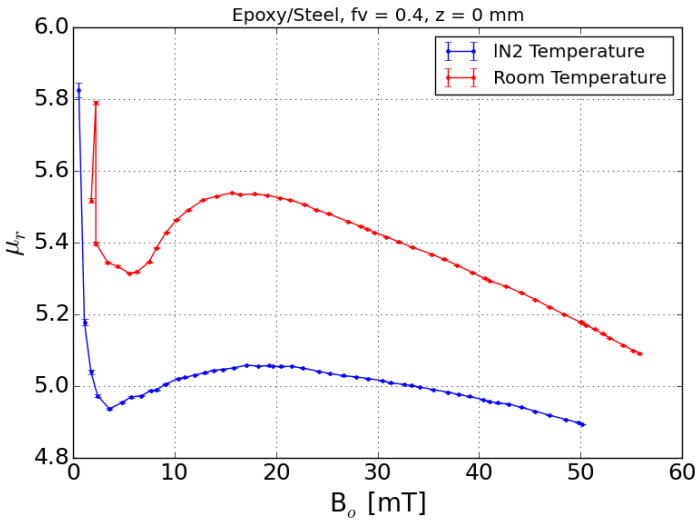

Figure 19: Comparison of the permeability of the steel/epoxy mixture (f=0.4) at room temperature and liquid nitrogen temperature. Note: the room temperature measurement is the same as in figure 18. The permeability of the ferromagnet reduces when subject to cryogenic temperatures. The larger permeability in the beginning likely results from the ferromagnet possessing an initial magnetization. The maximum at around 20 mT may suggests that the ferromagnet is beginning to saturate.

(a)

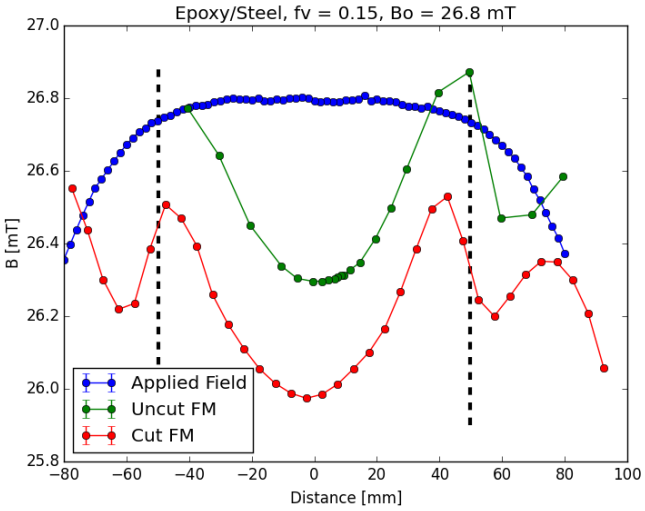

(b)

Figure 20: The internal length of a ferromagnet (f=0.15) subject to a Helmholtz field (blue curve) through the ferromagnet's length. Having maximum ferromagnetic shielding in the middle of the steel/epoxy mixture, i.e., reaching a minimum field near z = 0 mm, demonstrates the uniformity of the steel powder in the epoxy. Having maximum shielding near z = 0 mm even after cutting the ferromagnet in half demonstrates that we can stitch two ferromagnetic tubes to make a longer tube.

3.4 Conclusion

To meet the condition for magnetic cloaking, we fine-tune ferromagnet's μ_r by changing the volume fraction of 430 stainless steel powder in epoxy. We can then adjust the thickness with a lathe to meet the requirements of equation 1. We now must measure μ_r at higher fields to determine the viability of our ferromagnet solution in accelerator conditions.

4 Achieving Magnetic Cloaking

A superconductor and ferromagnet layer were combined to form a magnetic cloak. The cloak's effects were then measured in a 10 mT field.

4.1 Building A Magnetic Cloaking

The cloak was formed from 4 layers of the wide superconductor tape and from the ferretic epoxy of f=0.4. The ferromagnet has an inner diameter of 1.25" and an outer diameter of 1.54". Unfortunately, the superconducting tape could not cover the inner diameter. While we patched superconducting tape together to cover any gaps, the shielding capabilities suffered significantly. We will measure magnetic cloaking at 50 mT (and eventually 0.5 T) when we make a ferromagnet mold with a smaller inner diameter.

4.2 Confirmation of Magnetic Cloak

Figures 21 and 22 show that while the individual superconductor and ferromagnet layers distort the field, their combined effects result in an outside field that closely matches the external field. Figure 21 shows the magnetic field across the cloak's center [B_y vs x; (y, z)=(0, 0) mm] and 1 mm away from the surface [B_y vs. x; (y, z)=(0, 40.1) mm]. The field outside of the ferromagnet and superconductor added up to a field close to the Helmholtz field, signifying that the distortion of both layers counteracted each other. Figures 22 shows the field along the cloak's length through the center [B_y vs. z; (x, y)=(0, 0) mm] and 1 mm away from the center [B_y vs. z; (x, y)=(40.1, 0) mm]. The ends of the cloak showed significant deviation from the reference field. These edge effects can be mitigated by making the cloak longer than the magnetic field.

In all of these measurements, the cloak's profile was closer to the ferromagnet's profile than it was to that of the superconductor. We can correct for this by reducing the outer radius with a lathe.

Overall, these results are very promising. Our efforts are currently focused on making our results extend to higher fields, up to 0.5 T.

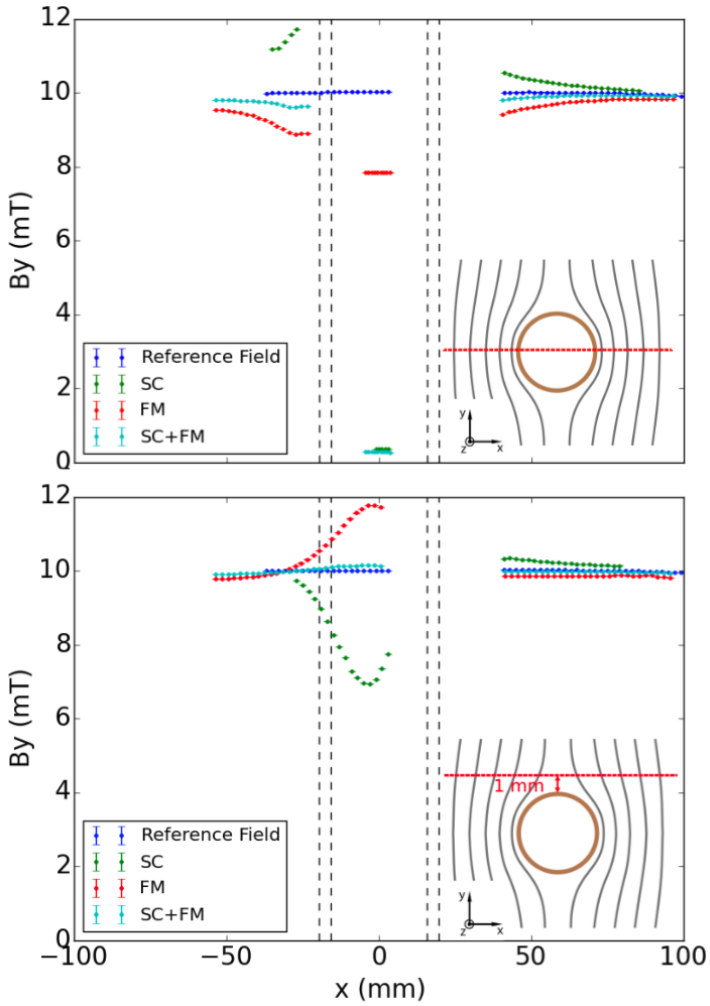

Figure 21: Measurements of the magnetic field B_y in y-direction created by a pair of Helmholtz coils with no objects inside the magnet (blue) and with a superconducting cylinder (green), a ferromagnetic cylinder (red), and a cloak (cyan) inside the magnet. These measurements cover multiple positions along the x-axis of the setup across the center of the cylinders (top figure) and 1 mm away from the cylinders (bottom figure). The dashed lines indicate the extensions of the cylinders. See inserts for axis orientations and lines of measurement w.r.t. the cylinders. The effects of the superconductor and the ferromagnet balance each other so that the combined field closely matches the applied field.

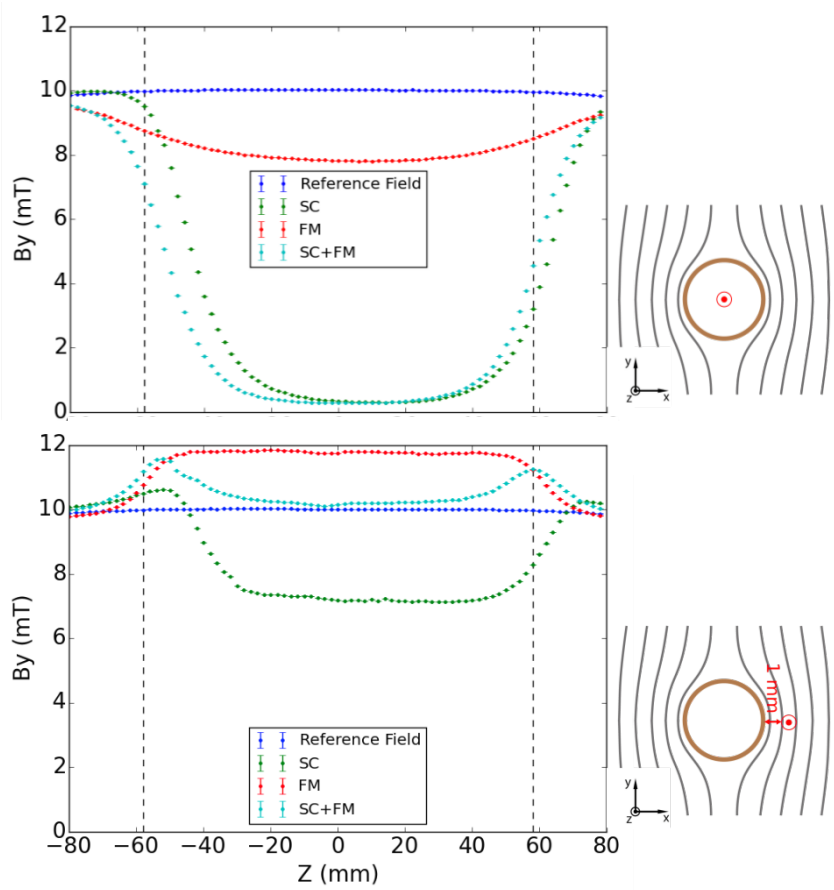

Figure 22: Measurements of the magnetic field B_y in y-direction created by a pair of Helmholtz coils with no objects inside the magnet (blue) and with a superconducting cylinder (green), a ferromagnetic cylinder (red), and a cloak (cyan) inside the magnet. These measurements cover multiple positions along the z-axis of the setup along the axis of the cylinders (top figure) and 1 mm away from the cylinders (bottom figure). The dashed lines indicate the extensions of the cylinders. See inserts for axis orientations and lines of measurement w.r.t. the cylinders. The cloak effectively shields its inside from magnetic fields at the center with fringe fields entering at the ends. While the superconductor and ferromagnet balance each other along most of the length of the cloak, significant fringe effects build up on the edges. These results motivate building a cloak that extends past the ends of the magnetic field.

5 Implementation of Cloak in Accelerator

Building a magnetic cloak to be used in a beam line is still a work in progress. We are still waiting to have access to a particle beam. In the meantime, we've built a 1.3 m cloak prototype, a cryostat to cool the superconductor while maintaining a vacuum of $\sim 10^{-6}$ Torr, and measured the field leakage throughout its length.

5.1 Cryostat Design

Cooling the superconductor in a beamline is more complicated than placing the superconductor in a liquid nitrogen bath. A vacuum must be maintained so that the beam does not get dissipated.

For our cryostat, we built a simple heat exchanger that will cool the superconductor through conduction. It is a 1 inch diameter liquid Nitrogen reservoir made from two connected copper tubes (figure 23b). The center is hollow and allows a beam to pass through. The cryostat has two 1/4 inch tube connections on both ends with a distance of 1.3 m. We wrapped five layers of superconductor tape covering a length of 1.3 m around the cryostat (figure 23c).

We assembled a test stand to commission the large prototype (for demonstrating the shielding of a charged particle beam from a magnetic field in the Van de Graaff accelerator) before installing it in the actual beam line. The test stand consists of a 2 m section of 4 inch beam pipe connected to a roughing pump and turbo pump, vacuum gauges, liquid Nitrogen feedthroughs, and electrical feedthroughs for temperature sensors and a Hall sensor (figure 23a).

To ensure a steady flow of liquid Nitrogen in the cryostat, we connected an open reservoir filled with liquid Nitrogen to one end of the cryostat and let the evaporating liquid Nitrogen gas flow out of the connection on the other end of the cryostat.

At a vacuum of 3×10^{-6} Torr and using 6 layers of mylar as heat radiation shield, the outside superconducting layer cooled down to 78.5 K after 4 hours.

5.2 Accelerator Prototype Shielding Performance

We measured the shielding performance of the 1.3 m superconductor shield prototype by adding five dipole magnets in series (figure 24). We attached a

(a)

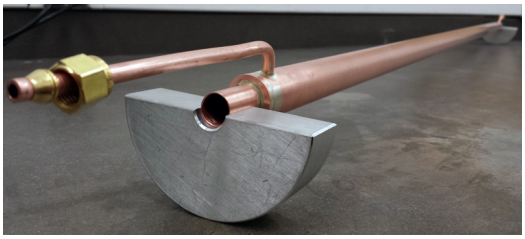

(b)

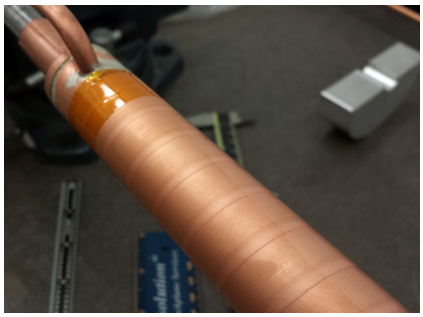

(c)

Figure 23: (a) The stand-alone test chamber for the large cloak prototype for the van de Graaf accelerator tests. (b) A simple heat exchanger cools the large prototype. The inside tube has an inner diameter of 0.561 inch, the outer tube has an outer diameter of 1 inch. (c) Superconductor tape wrapped in a helix around the cryostat.

Hall sensor to a 6" aluminum rod. The end of the rod exits the beam pipe section through a feedthrough, so that we can move the Hall probe while the beam tube remains evacuated. This setup allowed us to characterize the magnetic field shielding of this prototype along its length.

Figure 25 shows a measurement of the magnetic field shielding performance of this prototype. The prototype shielded the applied external field of 5 mT to 7 mT over 40 cm of the measured length, while the other section showed is a significant leakage of magnetic field though the superconductor. We are still investigating the source of this leakage. Possible reasons are a temperature gradient along the cryostat which brings the right end of the superconductor closer to the critical temperature then the left end, or gaps in the helix wrapping of the superconductor tape layers.

Figure 24: We attach 5 dipole magnets in series to test magnetic shielding along the length.

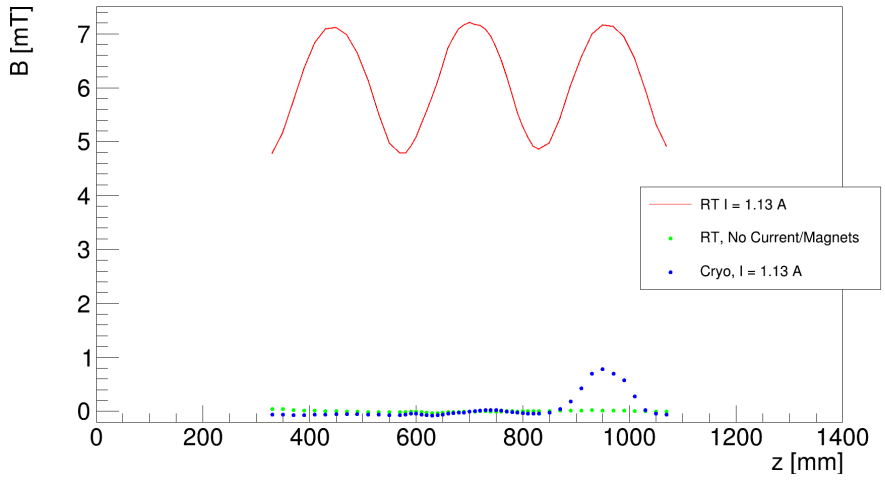

Figure 25: Measurement of the magnetic field B transverse to the center axis of our long prototype inside the beam pipe segment as a function of the position z along this axis. The red line shows the magnetic field of the five magnets at the chosen operating current (no superconductor shielding, room temperature). The green markers show the measurement of the magnetic field along the same line at room temperature when no external magnetic field is applied. The blue markers represent the measurement of the magnetic field after cooling the superconductor shield to liquid Nitrogen temperatures and switching on all five dipole magnets.

6 Summary and Further Work

In this work, we have:

1. Achieved magnetic shielding at 50 mT.
2. Established a methodology to predict shielding performance of multi-layer superconductor.
3. Demonstrated the ability to fine-tune the ferromagnet layer to achieve magnetic cloaking.
4. Demonstrated magnetic cloaking.

The next steps to realizing a magnetic cloak at the EIC include:

1. Demonstrating cloaking at 0.5 T. This is mostly a matter of finding the appropriate magnet.
2. Determining the radiation hardness of ferromagnetic and superconducting material.
3. Determining if the thermal effects due to an accidental beam dump can damage the cloak structure.
4. Quantify the physics benefit for a forward dipole magnet. What nuclear physics would we better measure?
5. What are the effects of the possible cryostat and its flanges on the detector acceptance and performance at small angle?

A How to Calculate Momentum Resolution

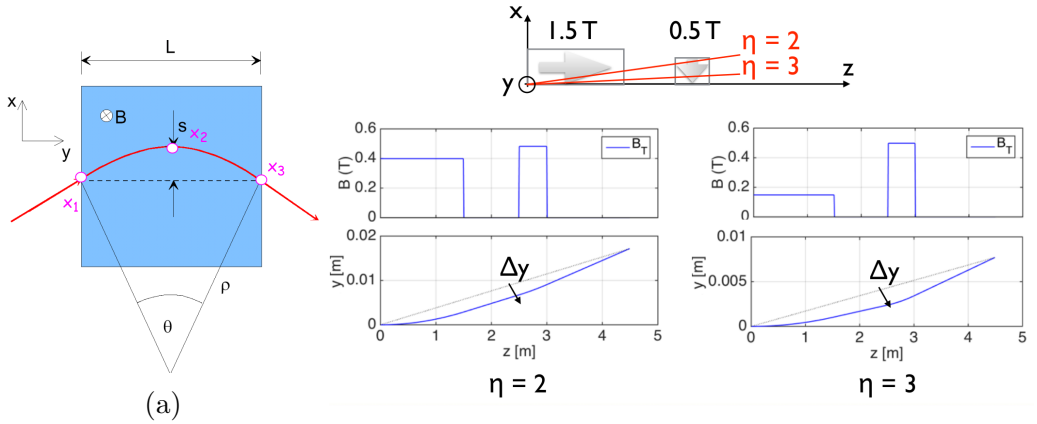

(a) (b)

Figure 26: Calculating the momentum kick of a 50 GeV charged particle in a solenoid + dipole field.

To calculate the momentum resolution, we follow these four steps[16]:

1. For the given magnetic field configuration and initial momentum, calculate the particles trajectory.

   From the Lorentz force law, we know that a charged particle going through a magnetic field will follow a circular trajectory. We can derive the relationship $p_T = qB\rho$, where q is the charge, B is the magnetic field, p_T is the momentum component transverse to the magnetic field, and ρ is the radius of the circular trajectory.

2. Calculate the sagitta of the trajectory.

   In an actual experiment, we don't measure ρ or the momentum, but the approximation of the trajectory based off of a distinct number of measuring stations. From the trajectory, we can measure the momentum kick ΔY (figure 26b). For a given z position, ΔY is the distance from the particles trajectory to the straight line connecting the end points of the trajectory's arc. We approximate this ΔY as the sagitta s of the arc. Knowing s allows us to calculate ρ and p_T:

$$s = \rho(1 - cos(\theta/2)) \approx \rho\theta^2/8 \approx \frac{0.3}{8}\frac{L^2 B}{p_T[GeV]}, \tag{4}$$

where L is the path length in the magnetic field.

3. From the space point resolution σ_x of your detector, calculate the uncertainty in the sagitta σ_s for three tracking stations.

$$\sigma_s = s\sqrt{(3/2)}\sigma_x \frac{8p_T}{0.3BL^2} \tag{5}$$

4. Equate the relative uncertainty in sagitta to the relative uncertainty in momentum.

$$\frac{\sigma_{p_T}}{p_T} = \frac{\sigma_s}{s} \tag{6}$$

B Other Possible Applications of a Magnetic Cloak

While this thesis focuses on developing the magnetic cloaking device in the context of placing it around a beamline, the applications are far broader. In general, one could place a magnetic cloak around instruments sensitive to magnetic fields without disturbing the magnetic fields themselves. For example, photomultiplier tubes are sensitive to magnetic fields because the photoelectrons will be deflected, changing the measured output[17]. A magnetic cloak can even be used to help maintain the polarization of helium during transport, which has far reaching applications from nuclear[18] to medical physics[19]. One might even place a magnetic cloak around a pacemaker to protect it during an MRI scan.

C Physics of Superconductors and Ferromagnets

Section 1.3 explains how one could use a superconductor and ferromagnet bilayer to achieve magnetic cloaking. There are many superconductors and ferromagnets to choose from, and the physics behind both materials is incredibly rich. Since deviations from the ideal cloak are expected, knowing the relevant physics behind both materials is essential for understanding the field measurements around the cloak and for picking the right materials to build the magnetic cloak.

C.1 Physics of Superconductors

Superconductors are materials that have zero electrical resistance when cooled below a critical temperature T_c. Superconductors act as perfect diamagnets. They prevent magnetic fields from penetrating their interior beyond the London penetration depth λ. This shielding is caused by surface currents that create a counter field which exactly cancels the applied field. Since magnetic fields do not penetrate an ideal superconductor, they can be used to shield objects inside of them from magnetic fields.

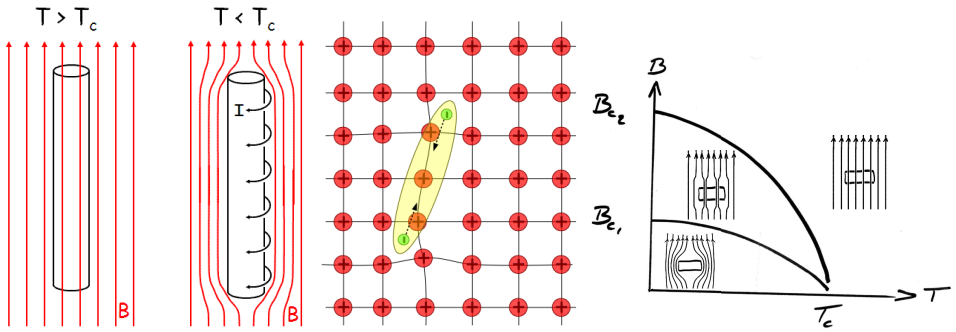

(a) [20] (b) [21] (c) [22]

Figure 27: (a) Superconductors shield their interiors from applied fields by creating currents to create counter-fields. (b) Superconductivity is caused by the formation of Cooper pairs. (c) Type-II superconductors have two critical fields. Between B_c1 and B_c2, field penetrates the interior through flux vortices, but the material still remains superconducting.

Superconductivity is caused by the interaction between electrons and the lattice of positive ions in a material. Electrons flying through the lattice cause lattice deformation, as electrons attract the positive ions and slightly displaces them. Another electron will then be attracted to this increase in positive charge distribution, leading to electron-electron coupling. This coupling leads to the formation of an electron pair known as a Cooper pair. Two fermions bound together effectively form a boson since two half-integer spins add to an integer spin. Since bosons are not subject to the Pauli exclusion principle, a large number of Cooper pairs can populate one collective state. Since all the Cooper pairs are in a collective state, scattering of one pair from the lattice atoms requires that the whole collective scatters as well. This just does not happen so there is no scattering of Cooper pairs. No scattering of

Cooper pairs leads to zero resistance.

In light of this mechanism, it is easy to understand why superconductivity only exists under a critical temperature and critical field. The coupling that leads to the formation of Cooper pairs is weak and can be destroyed by thermal motion of the lattice. The Cooper pairs can also be destroyed by the energy density associated with a magnetic field. Thus, even if we are below T_c, superconductivity cannot exist beyond a critical field B_c. The critical field B_c also sets a limit to the maximum superconductive current that can flow through the superconductor. Since current creates magnetic fields, the critical current I_c corresponds to the current that would create the critical magnetic field.

To achieve the best magnetic field shielding, we want to achieve the highest B_c possible. Since thermal energy and magnetic energy contribute to the destruction of Cooper pairs, we want to reduce the temperature as much as possible to increase B_c. B_c is related to the temperature by

$$B_c(T) = B_c(T = 0)(1 - (T/T_c)^2[11] \tag{7}$$

Superconductors have different magnetic properties, depending on whether they are type-I or type-II superconductors. Type-I superconductors are characterized by one critical field B_c. Below B_c, magnetic fields do not penetrate the superconductor. Above B_c, superconductivity is destroyed and magnetic field is no longer repelled. Type-II superconductors are characterized by two critical fields B_{c1} and B_{c2}. Below B_{c1}, the superconductor repels all magnetic fields. Between B_{c1} and B_{c2}, flux vortices form. These flux vortices act as regions of the normally conductive material and allow the magnetic field to partially penetrate the surface. Because the amount of normally conductive material increases as the field increases, more field penetrates with increasing external field. Beyond B_{c2}, the superconductivity is destroyed and the material becomes normally conductive[11].

Real superconductors have defects in their crystal structure that surprisingly improve their properties. Without defects, the vortices of a type-II superconductor repel each other and arrange themselves in a regular hexagonal pattern. However, if there are defects with size comparable to the flux vortices, then the vortices are pinned to these defects (the defects act as an energy local minimum). Because of pinning, the vortices can be arranged in a non-uniform spatial distribution. A nonequilibrium gradient in vortex density corresponds to an overall gradient in the field, which through Ampere's

law ($\nabla \times \mathbf{B} = \mu_0 \mathbf{J}$), corresponds to a current running through the bulk of the material instead of just the surface. The ability to carry a bulk current as opposed to just Meissner currents vastly increases a superconductors critical current, and consequently increases the critical field. A consequence of vortex pinning is that the thicker the superconductor, the more current it can carry and the more field it can shield. However, thermal excitation causes the vortices to escape their pinning sites and move to equilibrium, causing flux creep. Thus, the critical current reduces approximately logarithmically over time [23]. Also, there lies a critical field B_{irr} between B_{c1} and B_{c2} in which pinning is no longer effective (≈ 5 T for YBCO superconductor, greatly reducing the superconductor's shielding capabilities [11, p. 45]).

One must also consider the microstructure of the superconductor, especially for high temperature superconductor (HTS). In polycrystalline, materials, one must distinguish between intragranular critical current density J_{cg} (the critical current density within the grain) and intergranular critical current density J_{ci} (the critical current density between the grains). The grains are only weakly linked, so $J_{ci} << J_{cg}$. Thus, magnetic fields will start penetrating between the grains before they start penetrating through the grains. To achieve the highest J_{ci} and consequently the best shielding, one must increase the size of the grains and minimize the misorientation between different c-axes of the different grains.

C.2 Physics of Ferromagnets

Ferromagnets are characterized by how they respond to a magnetic field $\mathbf{H}$. In a field, the ferromagnet will obtain a magnetization $\mathbf{M}$. Both $\mathbf{M}$ and $\mathbf{H}$ determine the magnetic flux density $\mathbf{B}$, i.e. the number of field lines per unit area, that goes through the ferromagnet, such that $\mathbf{B} = \mu_0(\mathbf{H} + \mathbf{M})$. The dependence of $\mathbf{B}$ on $\mathbf{H}$ can be expressed as $\mathbf{B} = \mu_0 \mu_r \mathbf{H}$, where μ_r is called the relative permeability.

Ferromagnetism is caused by unpaired electrons in materials. These unpaired electrons have a net magnetic moment, and these moments couple with each other to align in the same direction[8]. However, if all the spins of a ferromagnet were aligned , a large magnetic field extending into the space outside itself would be created. A lot of magnetostatic energy would be

[8]The mechanism for this spin alignment is called the exchange interaction. Electrons repel each other and want to be far apart from each other. By having parallel spins, electrons do not occupy the same space because of the Pauli exclusion principle.

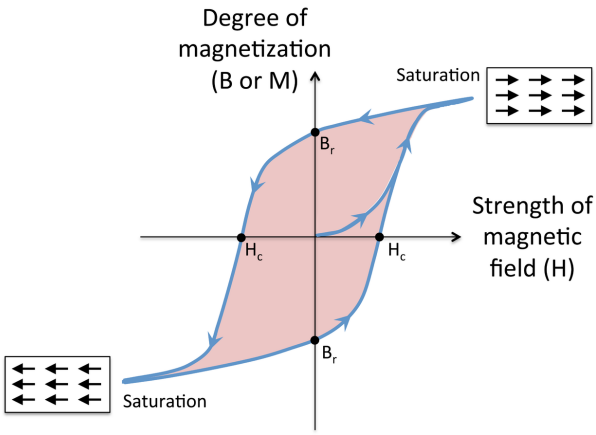

Figure 28: Magnetic hysteresis loop of a ferromagnet[24].

stored in this field. To minimize the internal field, domains form to give the ferromagnet material a zero net magnetization (in the absense of magnetic fields[9]). In the presence of magnetic fields, the domains with spins parallel to the field grow at the expense of other domains pointing in another direction.

When we apply a magnetic field to a ferromagnet, the ferromagnet gains a magnetization in a non-linear manner. As we increase $\mathbf{H}$, $\mathbf{B}$ increases slowly, then more rapidly, and then finally leveling off at the saturation field $\mathbf{B}_s$ when all the domains align with $\mathbf{H}$. Since μ_r is the slope of the B-versus-H curve, μ_r also depends on the magnetic field and essentially signifies how easy it is to magnetize a material. This process is not reversible. The domains resist movement in the opposite direction when the field is reversed. The response of $\mathbf{B}$ lags behind $\mathbf{H}$, leading to hysteresis. Thus, some remnant magnetization B_r remains after the $\mathbf{H}$ is removed.

The parameters that define a ferromagnets response to external fields is material dependent. Some parameters only depend on the material, regardless of its structure. For example, B_s depends on the density of unpaired electrons in a material. However, many properties such as μ_r and B_s are dependent on material structure. There are a variety of factors that affect the μ_r and B_r, including the fabrication method, impurities, and physical stresses[25, ch. 2]. The material structure affects how easily domains can align themselves with the magnetic field and how likely domains will maintain their alignment even after the field has been removed. The harder it

[9]Ignore hysteresis for now

is for domains to move, the lower μ_r is and the higher B_r is. Likewise, the easier it is for domains to move, the higher permeability and the lower the remnant field is.

D Long-term magnetic field shielding

Because of the flux creep mentioned in appendix C, a type-II superconductor's shielding capabilities will decay over time. We want to know the long term shielding behavior. We choose six months because that's how long collider experiments run. It is impractical to measure the shielding performance for six months, so we must extrapolate from a shorter measurement run. For proper extrapolation we must decide:

1. What function(s) do we model the time dependence of our data?
2. How long should we measure shielding to obtain a reliable extrapolation for 1/2 year.

D.1 How do we model the time dependence of our data?

There are many models in the literature that approximate magnetic relaxation of type-II superconductors, such as the Anderson and Kim model and the interpolation formula[23]. Unfortunately, all of these models undershoot the long-term field leakage of our measurements, i.e., fitting these models to the beginning portion of our data results in an extrapolated leaked field smaller than what we measure. This inconsistency probably manifests itself because our superconductor system is more complicated than the physical systems these models apply to. Our system is polygranular and the crystal axis has a different orientation to the magnetic field depending on where the grain is in the superconducting tube.

Thus, we extrapolate the long-term behavior by using two functions: one that always undershoots the long-term behavior and one that always overshoots. Empirically, we found that the logarithmic law, $Aln(\frac{t+1+c}{b})$ always undershot the long term behavior (figure 29a) while the power law, $a(t+c)^b$ overshot it (figure 29b). We see these two fits converge as we increase the experiment's run time.

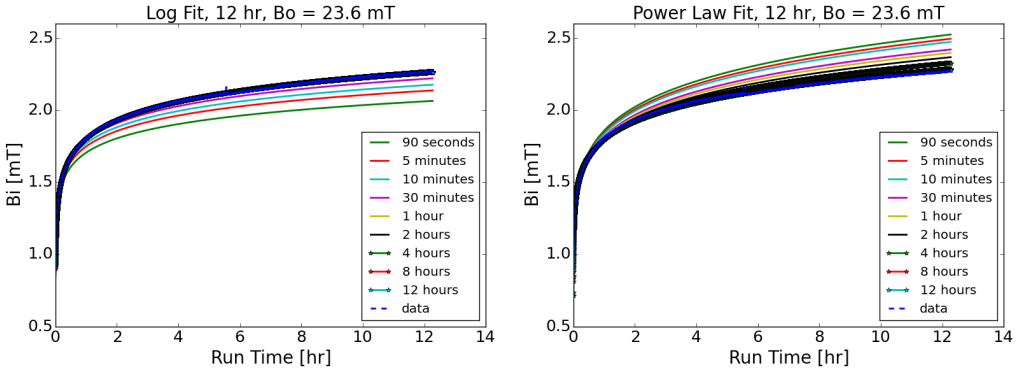

(a) (b)

Figure 29: A 12 hour measurement of the leaked field. A logarithm and power function were fitted to the beginning of the data to determine how well each function estimates the long-term value. (a) A logarithmic function always undershoots the long term behavior. (b) A power function always overshoots the long term behavior. Heuristically, the long-term leaked field is quoted as the average of the two models.

D.2 How long do we need to measure shielding to get a reliable extrapolation to 1/2 year?

After fitting the two functions, we say that the uncertainty is the span between the two curves. We find that the uncertainty decreases exponentially the longer our run time is. We ultimately chose ten minutes for most of our subsequent experiments to obtain a balance between reduced uncertainty and faster measurements.

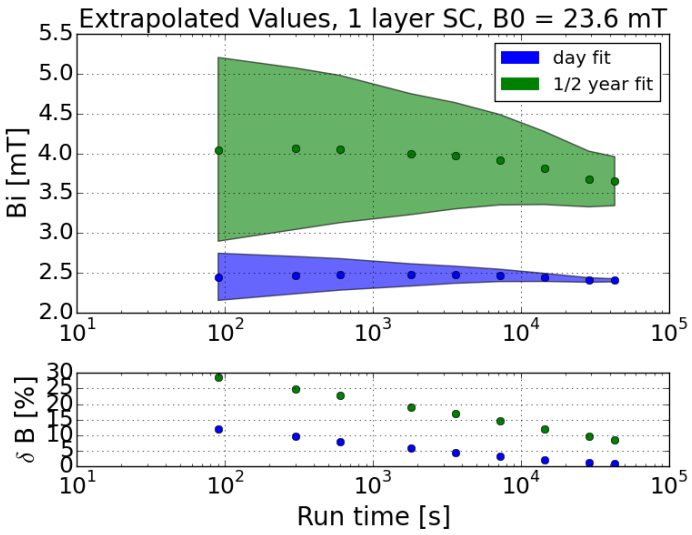

Figure 30: The average of the power and logarithm fits as a function of run time. The two models converge with longer run times.

References

[1] A. Accardi, J. Albacete, M. Anselmino, N. Armesto, E. Aschenauer *et al.*, "Electron Ion Collider: The Next QCD Frontier - Understanding the glue that binds us all," 2012.

[2] F. Gomory, M. Solovyov, J. Souc, C. Navau, J. Prat-Camps, and A. Sanchez, "Experimental realization of a magnetic cloak," *Science*, vol. 335, pp. 1466–1468, March 2012.

[3] I. Itoh, K. Kazuo, and O. Hiroaki, "Nbti/nb/cu multilayer composite materials for superconducting magnetic shielding-superconducting performances and microstructure of nbti layers-," Nippon Steel, Tech. Rep.

[4] J. Rabbers, M. Oomen, G. Riparmonti, and G. Giunchi, "Magnetic shielding capability of mgb2 cylinders," *Superconductor Science and Technology*, vol. 23, Dec 2010.

[5] Can Superconductors, "Bi-2223 magnetic shields," 2015. [Online]. Available: "http://www.can-superconductors.com/magnetic-shields.html"

[6] M. W. Rupich, X. Li, C. Thieme, S. Sathyamurthy, S. Fleshler, D. Tucker, E. Thompson, J. Schreiber, J. Lynch, D. Buczek, K. DeMoranville, J. Inch, P. Cedrone, and J. Slack, "Advances in second generation high temperature superconducting wire manufacturing and r&d at american superconductor corporation," *Superconductor Science and Technology*, vol. 23, no. 1, p. 014015, 2010. [Online]. Available: http://stacks.iop.org/0953-2048/23/i=1/a=014015

[7] N. Nouri and B. Plaster, "Comparison of magnetic field uniformities for discretized and finite-sized cos, solenoidal, and spherical coils," *Nuclear Instruments and Methods in Physics Research*, vol. 723, pp. 30–35, May 2013.

[8] S. Denis, L. Dusoulier, M. Dirickx, P. Vanderbemden, R. Cloots, M. Ausloos, and B. Vanderheyden, "Magnetic shielding properties of high-temperature superconducting tubes subjected to axial fields," *eprint arXiv:cond-mat/0701238*, Jan. 2007.

[9] J.-F. Fagnard, M. Dirickx, M. Ausloos, G. Lousberg, B. Vanderheyden, and P. Vanderbemden, "Magnetic shielding properties of high- tc superconducting hollow cylinders: model combining experimental data for axial and transverse magnetic field configurations," *Superconductor Science and Technology*, vol. 22, no. 10, p. 105002.

[10] I. Itoh, T. Sasaki, S. Minamino, and T. Shimizu, "Magnetic shielding properties of nbti/nb/cu multilayer composite tubes," *Applied Superconductivity, IEEE Transactions on*, vol. 3, March 1993.

[11] S. Denis, "Magnetic shielding with high-temperature superconductors," Master's thesis, Universite de Liege.

[12] K. N. Rozanov, A. Osipov, D. Petrov, S. Starostenko, and E. Yelsukov, "The effect of shape distribution of inclusions on the frequency dependence of permeability in composities," *Journal of Magnetism and Magnetic Materials*, vol. 321, no. 7, pp. 738–741, 2008.

[13] A. Sihvola and I. Lindell, "Effective permeability of mixtures," *Progress in Electromagnetic Research*, vol. 6, pp. 153–180, 1992.

[14] A. Zangwill, *Modern Electrodynamics*, 2012.

[15] "Magnetic properties of stainless steels at room and cryogenic temperatures," *Journal of Magnetism and Magnetic Materials*, vol. 321, no. 14, pp. 2107 – 2114, 2009, current Perspectives: Modern Microwave Materials.

[16] C. Niebuhr, "Momentum measurement in magnetic field lecture notes," lecture notes. [Online]. Available: http://graduierten-kurse.physi.uni-heidelberg.de/WiSe2007/lectures/Tracking/Lecture_2.pdf

[17] "Magnetic field effects on the photocathode uniformity of hamamatsu {R7081} photomultiplier tubes," *Nuclear Instruments and Methods in Physics Research Section A: Accelerators, Spectrometers, Detectors and Associated Equipment*, vol. 697, pp. 46 – 51, 2013.

[18] C. Epstein and R. Milner, "Development of a polarized 3he ion source for rhic using the electron beam ion source."

[19] J. M. Wild, J. Schmiedeskamp, M. N. J. Paley, F. Filbir, S. Fichele, L. Kasuboski, F. Knitz, N. Woodhouse, A. Swift, W. Heil, G. H. Mills, M. Wolf, P. D. Griffiths, E. Otten, and E. J. R. van Beek, "Mr imaging of the lungs with hyperpolarized helium-3 gas transported by air," *Physics in Medicine and Biology*, vol. 47, no. 13, p. N185.

[20] Hoffman Lab, "Superconductivity." [Online]. Available: http://hoffman.physics.harvard.edu/materials/SCintro.php

[21] M. N. Chernodub, "Electromagnetic superconductivity of vacuum induced by strong magnetic field," *Lect. Notes Phys.*, vol. 871, pp. 143–180, 2013.

[22] W. Commons, "The b-t diagram of type-ii superconductor." 2011.

[23] Y. Yeshurun, A. P. Malozemoff, and A. Shaulov, "Magnetic relaxation in high-temperature superconductors," *Rev. Mod. Phys.*, vol. 68, pp. 911–949, Jul 1996.

[24] Wikibooks, "Introduction to inorganic chemistry/metals and alloys: Structure, bonding, electronic and magnetic properties."

[25] R. Bozorth, *Ferromagnetism*, 1951.